Excitation of Plasmonic Waves in Graphene by Guided-Mode Resonances

Weilu Gao, Jie Shu, Ciyuan Qiu, and Qianfan Xu*

Department of Electrical and Computer Engineering, Rice University, Houston, Texas 77005, United States

ABSTRACT We propose an active plasmonic device based on graphene. Highly confined plasmonic waves in monolayer graphene are efficiently excited using an etched diffractive grating on silicon. The guided-wave resonance of the combined structure creates a sharp notch on the normal-incidence transmission spectra, as the incident optical wave couples to the graphene plasmonic wave. This structure can be used as a highly tunable optical filter or a broad-band modulator because the resonant wavelength can be quickly tuned over a wide wavelength range by a small change in the Fermi energy level of the graphene. In this paper, we analyze the performance of this device with finite-difference time-domain simulations. We compare the proposed structure with recently demonstrated graphene nanoribbons based on bound plasmonic oscillations.

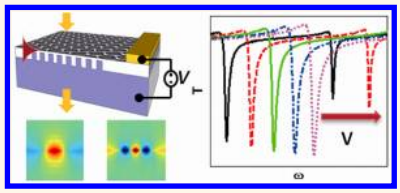

KEYWORDS: active plasmonics · graphene plasmonics · nanophotonics · mid-infrared devices · optoelectronics · tunable filters

The unique electronic properties of graphene[1−3] make it a promising platform to build highly integrated active plasmonic devices and systems for a wide wavelength range from near-infrared to THz.[4−9] Active plasmonics is an emerging field that allows manipulation and external control of light confined in a structure with deeply subwavelength dimensions. Existing active plasmonic devices have either slow speeds[10] or very limited tunability.[11,12]

In principle, the free carrier (electron or hole) density in a semiconductor can be adjusted by several orders of magnitude, resulting in a dramatic change in its plasmonic properties. This would allow strong control of plasmonic waves with an ultrabroad tunability. Unfortunately, at room temperature and high carrier density, the carrier mobilities in conventional semiconductors are too low to support plasmonic waves with useful propagation distances. In comparison, the carrier mobility in graphene remains high even at room temperature and at high carrier concentrations. Thus, the highly confined plasmonic wave can propagate many micrometers in the graphene film, which is ∼100 times the spatial period of the plasmonic wave in graphene at mid-IR frequencies.[4] The carrier density in graphene can be electrically adjusted by over 2 orders of magnitude with a small bias voltage applied on a field-effect transistor (FET),[6,13] which can achieve tuning time below a nanosecond.[14] This unique combination makes graphene the most promising material for highly tunable active plasmonic devices.

Besides the broad tunability, the plasmonic waves in graphene have extremely high field confinement. Theoretical studies show that the electric field of a mid-infrared plasmonic wave is localized in a layer a few tens of nanometers thick, 2 orders of magnitude smaller than its vacuum wavelength.[4] The highly localized optical field creates strong light−matter interactions[8] and can be used to build sensors with high sensitivity or to build nonlinear optical devices with high efficiency.[15] The plasmonic wave also has a low group velocity (∼c/100) over a wide wavelength range,[4] which allows for further enhancement of light−matter interaction as waves propagate slowly through the media.

Despite the impressive capabilities predicted theoretically, a key challenge is to efficiently couple to this plasmonic wave, given that its wavevector is much larger than that of free-space waves. While plasmonic effects in graphene have recently been demonstrated in graphene ribbons,[6] it resulted from plasmonic oscillations bounded by the ribbon instead of propagating plasmonic waves in a continuous graphene layer.

In this paper, we propose to use diffractive gratings to create a guided-wave resonance[16,17] in the graphene film that can be directly observed from the normal-incidence transmission spectra. The guided-mode resonance couples the normal-incidence optical waves to the plasmonic wave propagating in-plane, thereby creating a strong change in the optical transmission at the

* Address correspondence to qianfan@rice.edu.

Received for review April 30, 2012 and accepted August 5, 2012.

Published online August 05, 2012
10.1021/nn301888e

resonant frequency. This type of structure allows us to measure the dispersion relationship and electro-optic property of the plasmonic waves in graphene. We will show that the grating acts as a highly tunable optical filter that can be tuned with a small change in the Fermi level of the graphene. This structure can be used to build ultrafast spatial light modulators with broad operation bandwidth and opens a way to build 2D plasmonic photonic circuits and metamaterials.[18] With different grating periods, devices working in mid-infrared (mid-IR), far-infrared, or terahertz (THz) wavelength range can be built.

RESULTS AND DISCUSSION

Plasmon Wave in Graphene. The electronic properties of monolayer graphene have been intensely investigated,[3] and recent theoretic analysis[4] has shown that highly confined plasmonic waves can propagate in the monolayer graphene. These waves result from periodic motion of electrons or holes along the wave propagation direction. At a mid-infrared wavelength, optical losses from interband transition and phonon-induced scattering can be suppressed when the graphene is properly doped.[4] Under this condition, the Drude model[4] applies and the dispersion relationship of the plasmonic wave for the transverse magnetic (TM) mode in a continuous monolayer graphene is approximately[4] (see Materials and Methods)

$$\beta(\omega) \approx \frac{\pi\hbar^2\varepsilon_0(\varepsilon_{r1}+\varepsilon_{r2})}{e^2E_f}\left(1+\frac{i}{\omega\tau}\right)\omega^2 \qquad (1)$$

where $\beta(\omega)$ is the in-plane wavevector in graphene, $\hbar$ is the reduced Planck constant, ε_0 is the vacuum permittivity, ε_{r1} and ε_{r2} are the dielectric constants of the materials above and below the graphene film, τ is the carrier relaxation time, and $E_f = \hbar v_f(\pi n)^{1/2}$ is the absolute value of the Fermi energy level, where n is the carrier density and $v_f \approx 10^6$ m/s is the Fermi velocity in graphene. The carrier relaxation time τ determines the carrier mobility μ in graphene as $\tau = \mu E_f/ev_f^2$. The monolayer graphene layer is modeled as a 2D electron gas which has a metal-like response to in-plane electric field and a dielectric-like response to the surface-normal electric field (see Materials and Methods). The plasmonic dispersion property in graphene is different from that in other types of 2D electron gases[3] due to the massless electrons in graphene.

The carrier mobility μ of graphene film ranges from ~1000 cm^2/(V·s) in chemical vapor deposition (CVD)-grown graphene[6] to 230 000 cm^2/(V·s) in suspended exfoliated graphene.[19] When using a moderate mobility of 10 000 cm^2/(V·s) and with E_f = 0.64 eV, the dispersion relationship of the plasmonic mode is plotted in Figure 1. One can see from the blue line that the plasmonic mode has a high effective index n_{eff} = Re(β)/k_0 in the mid-IR wavelength range, which

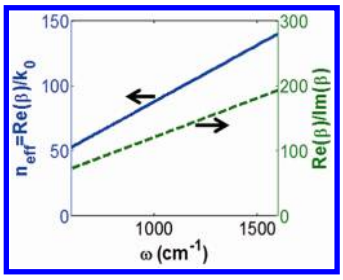

Figure 1. Dispersion property of the mid-infrared plasmonic waves in a monolayer graphene film with μ = 10 000 cm^2/(V·s) and E_f = 0.64 eV. The blue line shows the effective index of the plasmonic mode, and the green dashed line shows the ratio between the propagation length and the spatial period of the mode. The frequency of the wave is measured by its vacuum wavevector.

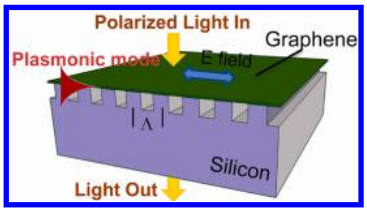

Figure 2. Schematics of a silicon diffractive grating-assisted graphene plasmonics excitation.

means the wavevector of the plasmonic wave is much larger than that of the incident wave. As a result, the electric field is highly confined, which will be shown later. The green line shows that the propagating length is 2 orders of magnitude longer than the spatial period of the plasmonic wave. This relatively low loss allows a high-Q and ultracompact resonator to be built.

Excitation by Diffractive Gratings. The large wavevector of plasmonic waves enables us to build devices with dimensions well beyond the diffraction limit. However, to excite the plasmonic wave in graphene with a free-space optical wave, their large difference in wavevector has to be overcome. Optical gratings are widely used to compensate wavevector mismatches. Here we use a silicon diffractive grating underneath the graphene, as shown in Figure 2, to facilitate the excitation. The grating is formed by patterning and etching shallow trenches on a silicon wafer. The grating period Λ needed for frequency ω_0 is determined by the phase match equation.

$$\mathrm{Re}(\beta(\omega_0)) - \frac{\omega_0}{c}\sin\theta = \frac{2\pi}{\Lambda} \qquad (2)$$

where c is the speed of light, θ is the incident angle, and ω_0/c is the vacuum wavevector k_0.

For a normal-incidence wave (θ = 0), a guided-wave resonance (GWR)[16,17] is excited when the grating period Λ matches the period of the plasmonic wave (2π/Re(β)) and the grating lines are perpendicular to the E-field direction of the incident wave. Under that condition, the normal-incidence wave excites the

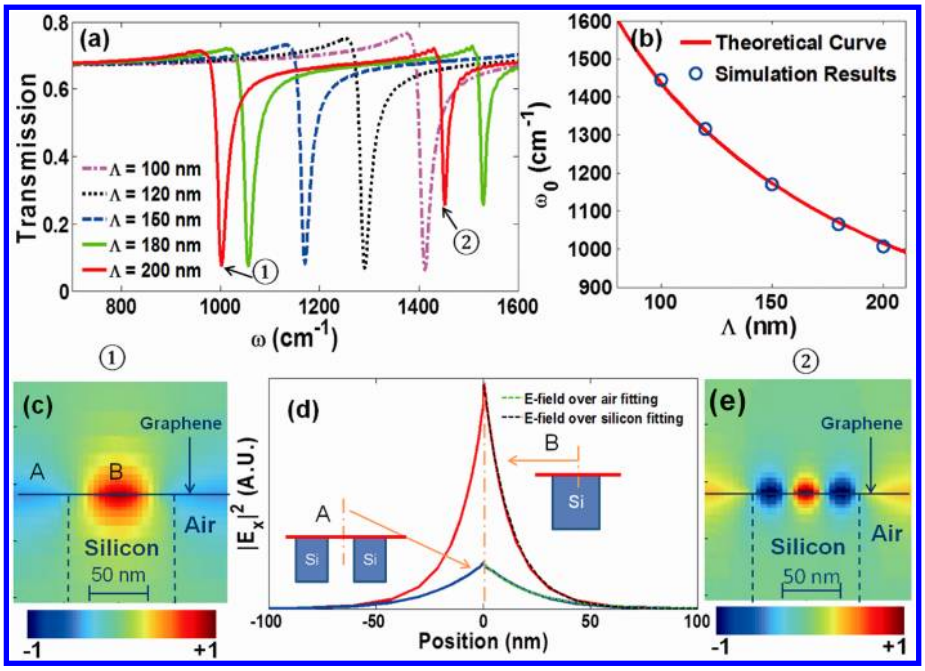

Figure 3. GWR in monolayer graphene on silicon gratings. (a) Simulated normal-incidence transmission spectra with different grating periods Λ for E_f = 0.64 eV. (b) Scaling of the fundamental-mode resonant frequency with respect to Λ. The dots are from the FDTD simulations, and the line is calculated from eq 3. (c) Side-view electrical field distribution of the fundamental mode in one grating period. (d) Distribution of the E-field intensity at the surface-normal direction along the two dash-dot lines that lies at the middle of a silicon ridge (red line) or an air gap (blue line). The black dashed line and green dashed line are exponential fittings to extract the decay lengths. (e) Side-view electric field distribution of the second-order mode in one grating period.

plasmonic wave in graphene and optical energy is dissipated due to the Ohmic loss while the plasmonic wave propagates in the graphene layer. Therefore, the transmission spectrum shows a notch around the resonant frequency ω_0 as

$$\omega_0 = \sqrt{\frac{2e^2 \times E_f}{\hbar^2 \varepsilon_0(\varepsilon_{r1} + \varepsilon_{r2})\Lambda}} \quad (3)$$

Here we simulate the optical response of the structure in Figure 2 using the finite-difference time-domain (FDTD) method. In the simulation, the graphene layer is modeled as an anisotropic electron gas with a thickness of 0.5 nm (see Materials and Methods).

The simulated normal-incidence transmission spectra with different grating periods (Λ) are shown in Figure 3a. One can indeed see sharp notches from the GWRs. The main notches have extinction ratios of ~10 dB and quality factors (Q) of ~40, which is larger than most metal mid-infrared resonance structures.[20−22] The scaling of the resonant frequency with respect to Λ agrees very well with eq 3, as shown in Figure 3b. On each transmission spectrum, one can identify multiple notches that result from multiple plasmonic modes. The side-view electric field profile of the fundamental mode in one grating period is shown in Figure 3c. The E-field has a 2π phase shift in each grating period, and the sign of the E-field flips at the edge of the silicon ribs. Figure 3d shows the E-field variations in the vertical direction at two horizontal positions, which are exponentially fitted, and the decay length is defined where the intensity drops to $1/e$ of the maximum intensity. Figure 3d confirms that the E-field is indeed tightly confined along the graphene layer with a decay length of 13.3 nm over the silicon ridges and 24.2 nm over the air trenches. The notches at the higher frequencies are caused by higher order modes. The electrical field profile of the second-order mode is shown in Figure 3e, where the E-field has a 4π phase shift in each grating period. The notch from the second-order mode can be minimized by adjusting the occupation ratio of the silicon grating.

The extinction ratio (ER) of the GWR notch in the transmission spectra is largely determined by the optical loss in graphene, which is mainly characterized by the real part of the conductivity at the operating mid-IR frequency.[23] While the electron mobility in an exfoliated graphene can exceed 230 000 $cm^2/(V \cdot s)$,[19] the CVD graphene generally has mobility below 10 000 $cm^2/(V \cdot s)$ due to the point defects and residue impurity introduced during growth or transfer of graphene. The lower mobility corresponds to higher loss and lower intrinsic Q for the GWR. Thus, the notches in the transmission spectra become broader and shallower. As shown in Figure 4a, when the mobility decreases to μ = 1000 $cm^2/(V \cdot s)$, the ER drops to a low but measurable level of ~20%.

In additional to the impurity-induced loss characterized by the Drude model, recent experiments[24−26]

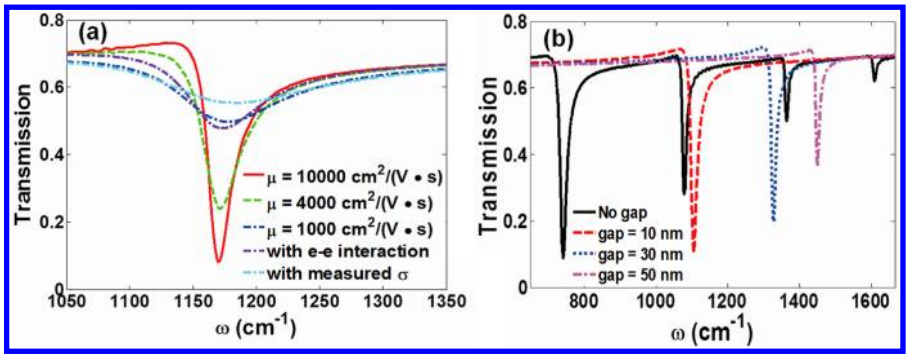

Figure 4. Simulated normal-incidence transmission spectra of monolayer graphene on silicon gratings. (a) Spectra with different carrier mobilities when E_f = 0.64 eV and Λ = 150 nm. The cyan dash-dot line and the purple dash-dot line show the simulated spectra with the measured conductivity[24] and with the modeled conductivity where the electron−electron interactions are taken into consideration.[25] (b) Spectra with different gaps between the graphene and the silicon grating when E_f = 0.64 eV on Λ = 370 nm and μ = 10 000 cm²/(V·s).

have shown additional losses in the infrared spectral range, where the measured real part of the conductivity is higher than that predicted by the Drude model and the DC mobility μ. We simulated the transmission spectrum of the device with the measured conductivity of graphene (see Materials and Methods),[24] which is shown as the cyan dash-dot line in Figure 4a. While the additional loss observed in experiments severely limits the ER of the proposed device (and the performance of graphene plasmonic devices in general),[23] it is not conclusive yet how much of this additional loss is from an intrinsic process such as the electron−electron interaction, and how much of it is from an extrinsic influence such as the defects and the substrate effect.[26−28] The electron−electron interaction is included in the model given in ref 25, and a simulation with results of that model (purple dash-dot line in Figure 4a) gives a better ER than that with the measured conductivity. Even though the electron−electron interaction is intrinsic, it can be tuned by using different substrates,[25] and recent measurements have shown that the propagation lengths of mid-IR plasmonic waves in graphene on SiC substrate agrees with what is predicted from the Drude model and the DC mobility.[28] Therefore, with a graphene of a higher quality,[29,30] a low-loss graphene plasmonic wave may be obtained in the future. In addition, the loss can possibly be compensated by an optical gain introduced through population inversion.[31,32]

Another factor that affects the ER is the strength of the gratings. To show that, we add a small air gap between the silicon grating and the graphene film, which reduces the overlap between the graphene plasmonic wave and the grating and thus reduces the effective strength of the grating. One can see in Figure 4b that the ER drops when the grating is moved farther away from the graphene film, but the extinction ratio remains high when the gap is less than 30 nm. The resonant frequency blue shifts as the gap increases because the effective index of the plasmonic mode becomes smaller. With such a gap, the silicon grating with a proper doping level can be used as the gate electrode to tune the Fermi level of graphene.[33] Since the distance between the gate electrode and the gap is typically just a few nanometers, the shape and the extinction ratio of the resonances will be very close to those without the gap. Given the fast carrier diffusion[34] and the small grating period, we expect the carrier distribution in graphene to be nearly uniform even though the gate electrode is patterned.

Electrostatic Tuning of the GWR. The most intriguing property of graphene plasmonics is its ultrabroad and fast tunability.[6] Electrical tuning of the notch filter shown above can be achieved by adjusting the Fermi level in graphene. Simulated spectra shown in Figure 5a confirm the broad tuning range with a small change in the Fermi level. The tuning curve agrees very well with eq 3, as shown in Figure 5b. The Fermi level in graphene can be controlled with potentially fast speed using an FET structure,[6] where the approximate relationship is $E_f \propto (V_g)^{1/2}$ and V_g is the gate voltage. It has been shown that a Fermi level change of 0.1 eV can be obtained with a gate voltage of a few volts,[6,33] which would induce the resonant frequency to shift ~100 cm^{-1}. Besides acting as a highly tunable optical filter, the fast tuning speed allows the structure to be used as a spatial light modulator for a wide frequency range from mid-IR to THz.

Besides the FDTD simulations, we also analyze the grating structure analytically with the rigorous coupled-wave analysis (RCWA) method (see Materials and Methods).[35] The results agree very well with the FDTD simulation, as shown in Figure 5b. The RCWA method is much quicker than the FDTD simulation and thus allows us to explore a wide design space quickly.

Bound Electron Oscillation in Graphene Nanoribbons. When a graphene film is patterned to a micrometer or nanometer dimension, the motion of the free carriers is restricted, which supports resonant oscillation modes as the bound electrons. This plasmonic oscillation in patterned graphene structures like graphene nanoribbon and disks[8] can also be excited by normal-incidence

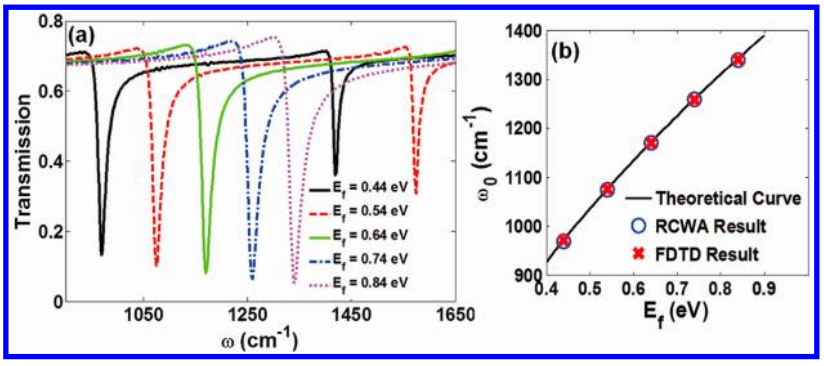

Figure 5. (a) Simulated normal-incidence transmission spectra of monolayer graphene on silicon gratings with different Fermi energy level in graphene when μ = 10 000 cm^2/(V·s) and Λ = 150 nm. (b) Scaling rule of resonant frequency with respect to E_f using both RCWA and FDTD methods. The dots and crosses are simulated results from RCWA and FDTD, respectively, and the line is calculated from eq 3.

free-space waves. The resonant behavior of micrometer-wide graphene ribbons at the THz spectral range has been demonstrated experimentally.[6] The observed optical spectra, which have similar features as those of the GWRs shown in the previous section, are due to the excitation of the bound electron oscillations in the isolated graphene structures. Here we analyze the optical effects of the plasmonic oscillation in graphene ribbon arrays using the FDTD method and compare that to the GWR that couples the free-space wave to the plasmonic waves in continuous graphene films. We will show that the plasmonic wave in continuous graphene excited by the GWR has better field confinement in the surface-normal direction than that of the graphene ribbons.

The bound electron oscillation in isolated graphene ribbons can be analyzed with a quasi-static analysis.[6] The resonant frequency ω_0 is determined by the width of the ribbon and the Fermi level as eq 5 if the damping is not large[6]

$$\omega_0 \cong \sqrt{\frac{e^2 \times E_f}{\hbar^2 \eta \varepsilon_r \varepsilon_0 w}} \cong 0.62\sqrt{\frac{e^2 \times E_f}{\hbar^2 \varepsilon_r \varepsilon_0 w}} \qquad (5)$$

where η is a dimensionless constant which can be deduced from our simulation results to be 2.63, w is the ribbon width, and ε_r is the dielectric constant of the surrounding medium. For simplicity, we assume that the graphene ribbons are suspended in the following simulations, so that ε_r = 1. One can see from eq 5 that the resonant frequency scales with the square root of the ribbon width. Thus, when the occupation ratio of a periodic ribbon array is fixed, the resonant frequency scales with the square root of the period. This is the same scaling rule as how the GWR scales with the grating period shown in the previous section.

The transmission spectra of the graphene ribbon array shown in Figure 6a are simulated with the FDTD method. Plasmon oscillation is excited when the electrical field of incident wave is perpendicular to the ribbons. As shown in Figure 6b, sharp resonance notches with ER ~ 15 dB and Q ~ 20 are observed when the graphene has a mobility μ = 10 000 cm^2/(V·s). The side-view E-field profile of the fundamental mode is shown in Figure 6c. Besides the singular peaks at the edges of the ribbon, the E-field distribution on the surface-normal direction is less confined than that of the GWR mode shown before. A decay length of 45 nm is measured from the vertical distribution across the center of the ribbon, as shown in Figure 6d. This decay length is three times longer than that of the GWR mode in continuous graphene. When the occupation ratio is fixed at 50%, the resonant frequency of the nanoribbon array scales as the square root of the repetition period, as shown in Figure 6e. Similar to the graphene on silicon gratings, the ER of the resonance decreases when the carrier mobility decreases, as shown in Figure 6f. Using our simulation tool, we can also fit very well the experimentally measured transmission spectrum in ref 6, as shown in Figure 6g. From the fitting, we determine that the mobility of graphene used in that experiment was 967 cm^2/(V·s), which is very close to the authors' claim.

Similar to the GWR shown above, the resonance of the graphene nanoribbons can be tuned when the Fermi level is changed. One can see from Figure 7 that the central frequency shifts with the Fermi level following the same scaling rule as the GWR denoted by eq 5.

Comparison between GWR and Nanoribbon Resonances. The analysis of resonant frequency shown above did not take into account the interactions between the plasmonic oscillations in neighboring ribbons.[36,37] When the ribbons are placed close to each other, the oscillation mode splits to an even mode where neighboring ribbons are in phase and an odd mode where neighboring ribbons are out of phase. For the odd mode, the radiations from neighboring ribbons destructively interfere at the far field in the vertical direction. Thus, this mode cannot be excited by the normal-incidence waves. Therefore, one can only

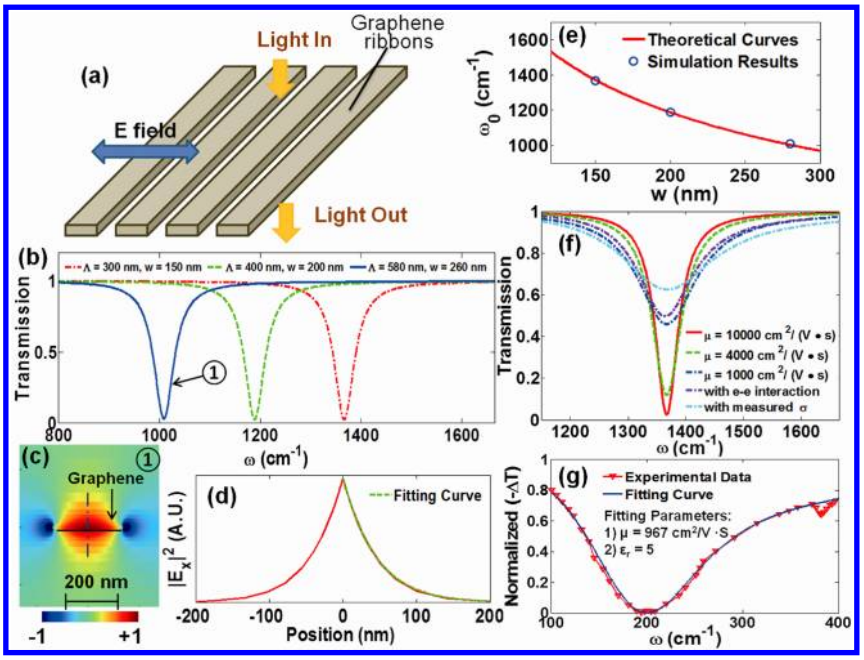

Figure 6. (a) Schematics of a graphene nanoribbon array to excite bound electron oscillation in graphene. (b) Simulated normal-incidence transmission spectra with different ribbon widths w and a fixed occupation ratio of 50%. (c) Side-view electrical field distribution of the fundamental mode in one period. (d) Red line is the distribution of the E-field intensity at the surface-normal direction along the dash-dot lines in (c) that lies at the center of the ribbon. The green dashed line is the exponential fitting to extract the decay length. (e) Scaling of the fundamental-mode resonant frequency with respect to w. The dots are from the FDTD simulations, and the line is calculated from eq 5. (f) Spectra with different carrier mobilities when E_f = 0.64 eV and Λ = 300 nm. The cyan dash-dot line and the purple dash-dot line show the simulated spectra with the measured conductivity[24] and with the modeled conductivity where the electron−electron interactions are taken into consideration.[25] (f) Red triangles are experimental results for an array of ribbons in ref 6, where w = 1 μm and E_f = 0.45 eV. The blue line is the simulated result with μ = 967 cm^2/(V·s) and ε_r = 5. The normalized spectrum $-\Delta T$ is defined by $-(T - T_{CNP})$, where T is the optical transmission and T_{CNP} is the transmission when the graphene is at the charge-neutral point.

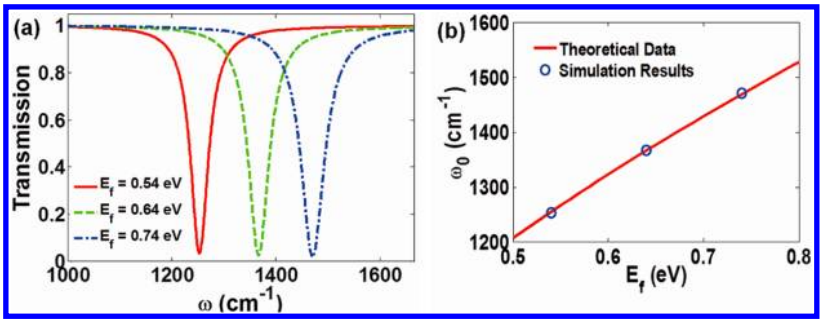

Figure 7. (a) Simulated normal-incidence transmission spectra of graphene ribbon array with different Fermi energy level in graphene when μ = 10 000 cm^2/(V·s) and w = 150 nm. (b) Scaling rule of resonance frequency with respect to E_f. The dots are simulated results from FDTD, and the line is calculated from eq 5.

observe one resonant notch on the transmission spectra, which is from the even mode. Figure 8a shows how the coupling between ribbons changes the resonance of the ribbon array. Here the width of the ribbons is fixed, while the period of the array, and thus the gap between the ribbons, is changed. The blue line in Figure 8b shows that the resonant frequency red shifts as the gap shrinks following an exponential dependency. This is caused by an exponential increase in the coupling strength between the ribbons as the gap decreases. When the gap between the ribbons is very wide, the resonant frequency approaches that of an individual graphene ribbon, which is marked as the dashed line in Figure 8b.

In comparison, the dielectric grating in the GWR structure excites plasmonic waves in a continuous graphene film, and the resonant frequency is mainly determined by the period of the grating. When the width of either the silicon ridges or the trenches between the ridges is fixed, the resonant frequency blue shifts as the period decreases. The scaling curves shown as the red squares and pink triangles in Figure 8b are similar to the scaling curve when

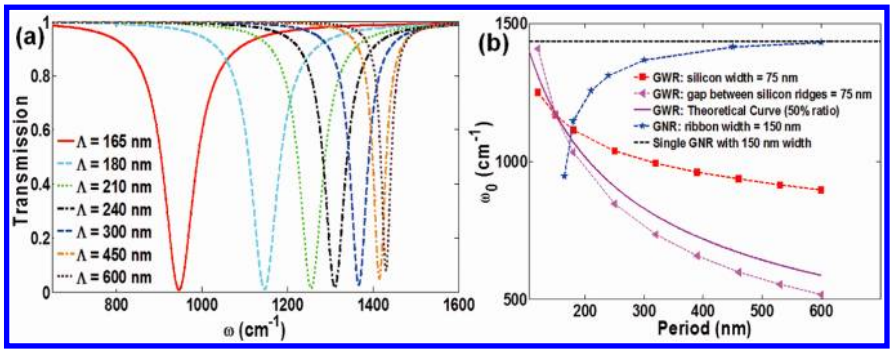

Figure 8. (a) Simulated normal-incidence transmission spectra of the graphene ribbon array when the ribbon width is fixed at 150 nm and the gap between ribbons varies. (b) Resonant frequency *versus* the repetition period of a silicon grating (GWR) or a nanoribbon array (GNR) when the ribbon width is fixed at 150 nm (blue stars), when the silicon ridge width is fixed at 75 nm (red squares), when the gap between the silicon ridges is 75 nm wide (pink triangle), and when the occupation ratio is fixed at 50% (purple line). The black dashed line marks the resonant frequency of a single graphene ribbon with a width of 150 nm.

occupation ratio is fixed (the solid purple line, same as the red line in Figure 3b). The differences between the three curves come from the change in the effective index of the plasmonic mode, which increases with the occupation ratio of the high-index material silicon.

One can clearly see in Figure 8b that the scaling rules for GWR are opposite to the scaling rule of the graphene ribbon array, which reveals the fundamental difference between these two structures. In the former case, the diffractive gratings act as a wavevector matching component to excite the plasmonic waves in the graphene layer, in which the grating period is the determinant factor for the resonant frequency. The resonances of the graphene ribbons are due to the bounded electron oscillation that is set mainly by the width of the ribbons.

CONCLUSION

We propose to use periodic diffractive grating structures to excite the highly confined plasmonic waves in monolayer graphene films. Numerical simulations confirm our theoretical analysis and give an insight of active plasmonic devices based on graphene. The proposed structure can be used to build an ultrafast spatial light modulator with broad operation bandwidths and to build 2D plasmonic photonic circuits and metamaterials.

MATERIALS AND METHODS

The proposed structures are simulated with the finite-difference time-domain method using Lumerical FDTD solutions. In the simulations, the graphene film is modeled as a thin layer with a thickness t = 0.5 nm and an anisotropic dielectric constant described by a diagonal tensor. The in-plane dielectric tensor component is $\varepsilon_{r11} = \varepsilon_{r22} = 2.5 + i\sigma/(\varepsilon_0\omega t)$, where σ is the conductivity of graphene, and the surface-normal component is set as $\varepsilon_{r33} = 2.5$ based on the dielectric constant of graphite. The simulation result does not change when the thickness t is set to a different value, such as 0.3 nm, as long as the mesh is fine enough. Since there is a large dimensional difference between the thickness of the graphene (0.5 nm) and the grating periods (on the order of 100 nm), we use non-uniform mesh in the FDTD simulations. The mesh size inside the graphene layer is 0.05 nm, and the mesh size gradually increases outside the graphene layer.

The only material property of graphene needed for the simulation is the conductivity spectrum over the simulated mid-IR frequency range. The intraband conductivity of graphene at mid-infrared frequencies is modeled with a semiclassical Drude model with a finite temperature correction[38] as

$$\sigma(\omega) = \frac{2e^2}{\pi\hbar^2} k_B T \times \ln\left[2 \times \cosh\left(\frac{E_f}{2k_B T}\right)\right] \frac{i}{\omega + i\tau^{-1}}$$

where k_B is the Boltzmann constant and T is the temperature. At room temperature and for Fermi level of interest, $E_f/2k_BT \gg 1$ and $\cosh(E_f/2k_BT) \approx 1/2e^{(E_f/2k_BT)}$, this equation is thus reduced to $\sigma(\omega) = i(e^2E_f/\pi\hbar^2)/(\omega + i\tau^{-1})$. Here the effect from the interband transition is neglected because the photon energy in the simulated spectral range is always less than $2E_f$. The simulations in the paper are performed at a frequency below the optical phonon frequency of 1667 cm^{-1}. When the frequency is higher than 1667 cm^{-1}, additional losses from an electron interacting with an optical phonon[3,4] can be incorporated with $\tau^{-1} = \tau_{imp}^{-1} + \tau_{el-ph}^{-1}$, where the τ_{imp} is the relaxation time from impurities in graphene and τ_{el-ph} is from electron−phonon coupling loss.

Additional simulations are performed using the conductivities from experimental measurements[24] and from a theoretical model[25] that takes into account electron−electron interactions, and the results are shown as the cyan and purple lines in Figures 4a and 6f. The measured conductivities in ref 24 are taken at $E_f \leq 0.3$ eV, while the simulation here is done at $E_f = 0.64$ eV, where the real part of the conductivity is expected to be higher. We observed that the measured real part of the conductivity in the frequency range of interest can be fitted very well as a sum of a Drude model part and a flat floor of $\sim 0.3\pi e^2/2h$, which is relatively independent of the Fermi level.[27] In our simulation, the conductivity at $E_f = 0.64$ eV is extrapolated from the measured data at $E_f = 0.3$ eV by scaling the Drude model part according to the equation above while keeping the flat floor part unchanged.

The dispersion relationship of TM polarized plasmonic waves in graphene is $\varepsilon_{r1}(\beta^2 - \varepsilon_{r1}k_0^2)^{-1/2} + \varepsilon_{r2}(\beta^2 - \varepsilon_{r2}k_0^2)^{-1/2} = -i\sigma/\omega\varepsilon_0$,[4] where k_0 is vacuum wavevector. Since the solution satisfies $\beta \gg k_0$, the previous equation can be reduced to the dispersion relationship as shown in eq 1.[4]

The rigorous coupled-wave analysis is also used to calculate the optical response of the structures. The RCWA solves the Maxwell equations and the boundary conditions based on the harmonic analysis where the grating structure is decomposed into different Fourier components. The details of this method can be found in ref 35.

The graphene Fermi level can be changed by applying a gate voltage. The approximate relationship can be estimated as a parallel capacitor. The capacitor-induced carrier concentration of the graphene is $n_g = \varepsilon_0\varepsilon_d V_g/ed$, and the Fermi level is $E_f = \hbar v_f(\pi n_g)^{1/2}$. Here the ε_d is the dielectric constant of the insulating layer and d is the thickness of insulating layer. Assuming that $\varepsilon_d = 4$ and $d = 2$ nm, it takes ~1 V to change the Fermi level from 0.54 to 0.64 eV.

Conflict of Interest: The authors declare no competing financial interest.

Acknowledgment. This work was partially supported by DOD: Air Force Office of Scientific Research (AFOSR) Grant FA9550-12-1-0261.

REFERENCES AND NOTES

1. Geim, A. K.; Novoselov, K. S. The Rise of Graphene. *Nat. Mater.* **2007**, *6*, 183–191.
2. Novoselov, K. S.; Geim, A. K.; Morozov, S. V.; Jiang, D.; Zhang, Y.; Dubonos, S. V.; Grigorieva, I. V.; Firsov, A. A. Electric Field Effect in Atomically Thin Carbon Films. *Science* **2004**, *306*, 666–669.
3. Castro Neto, A. H.; Guinea, F.; Peres, N. M. R.; Novoselov, K. S.; Geim, A. K. The Electronic Properties of Graphene. *Rev. Mod. Phys.* **2009**, *81*, 109–162.
4. Jablan, M.; Buljan, H.; Soljacic, M. Plasmonics in Graphene at Infrared Frequencies. *Phys. Rev. B* **2009**, *80*, 245435.
5. Mishchenko, E. G.; Shytov, A. V.; Silvestrov, P. G. Guided Plasmons in Graphene P-N Junctions. *Phys. Rev. Lett.* **2010**, *104*, 156806.
6. Ju, L.; Geng, B. S.; Horng, J.; Girit, C.; Martin, M.; Hao, Z.; Bechtel, H. A.; Liang, X. G.; Zettl, A.; Shen, Y. R.; *et al.* Graphene Plasmonics for Tunable Terahertz Metamaterials. *Nat. Nanotechnol.* **2011**, *6*, 630–634.
7. Bao, Q. L.; Zhang, H.; Wang, B.; Ni, Z. H.; Lim, C. H. Y. X.; Wang, Y.; Tang, D. Y.; Loh, K. P. Broadband Graphene Polarizer. *Nat. Photonics* **2011**, *5*, 411–415.
8. Koppens, F. H. L.; Chang, D. E.; de Abajo, F. J. G. Graphene Plasmonics: A Platform for Strong Light−Matter Interactions. *Nano Lett.* **2011**, *11*, 3370–3377.
9. Rana, F. Graphene Terahertz Plasmon Oscillators. *IEEE Trans. Nanotechnol.* **2008**, *7*, 91–99.
10. Pala, R. A.; Shimizu, K. T.; Melosh, N. A.; Brongersma, M. L. A Nonvolatile Plasmonic Switch Employing Photochromic Molecules. *Nano Lett.* **2008**, *8*, 1506–1510.
11. MacDonald, K. F.; Samson, Z. L.; Stockman, M. I.; Zheludev, N. I. Ultrafast Active Plasmonics. *Nat. Photonics* **2009**, *3*, 55–58.
12. Dionne, J. A.; Diest, K.; Sweatlock, L. A.; Atwater, H. A. PlasMOStor: A Metal-Oxide-Si Field Effect Plasmonic Modulator. *Nano Lett.* **2009**, *9*, 897–902.
13. Schwierz, F. Graphene Transistors. *Nat. Nanotechnol.* **2010**, *5*, 487–496.
14. Liu, M.; Yin, X.; Ulin-Avila, E.; Geng, B.; Zentgraf, T.; Ju, L.; Wang, F.; Zhang, X. A Graphene-Based Broadband Optical Modulator. *Nature* **2011**, *474*, 64–67.
15. Mikhailov, S. A. Theory of the Giant Plasmon-Enhanced Second-Harmonic Generation in Graphene and Semiconductor Two-Dimensional Electron Systems. *Phys. Rev. B* **2011**, *84*, 045432.
16. Rosenblatt, D.; Sharon, A.; Friesem, A. A. Resonant Grating Waveguide Structures. *IEEE J. Quantum Electron.* **1977**, *33*, 2038–2059.
17. Sharon, A.; Glasberg, S.; Rosenblatt, D.; Friesem., A. A. Metal-Based Resonant Grating Waveguide Structures. *J. Opt. Soc. Am. A* **1997**, *14*, 588–595.
18. Vakil, A; Engheta, N. Transformation Optics Using Graphene. *Science* **2011**, *332*, 1291.
19. Bolotin, K. I.; Sikes, K. J.; Jiang, Z.; Klima, M.; Fudenberg, G.; Hone, J.; Kim, P.; Stormer, H. L. Ultrahigh Electron Mobility in Suspended Graphene. *Solid State Commun.* **2008**, *146*, 351–355.
20. Wu, C. H.; Khanikaev, A. B.; Adato, R.; Arju, N.; Yanik, A. A.; Altug, H.; Shvets, G. Fano-Resonant Asymmetric Metamaterials for Ultrasensitive Spectroscopy and Identification of Molecular Monolayers. *Nat. Mater.* **2012**, *11*, 69–75.
21. Verellen, N.; Dorpe, P. V.; Huang, C. J.; Lodewijks, K.; Vandenbosch, G. A. E.; Lagae, L.; Moshchalkov, V. V. Plasmon Line Shaping Using Nanocrosses for High Sensitivity Localized Surface Plasmon Resonance Sensing. *Nano Lett.* **2011**, *11*, 391–397.
22. Fedotov, V. A.; Rose, M.; Prosvirnin, S. L.; Papasimakis, N.; Zheludev, N. I. Sharp Trapped-Mode Resonances in Planar Metamaterials with a Broken Structural Symmetry. *Phys. Rev. Lett.* **2007**, *99*, 147401.
23. Tassin, P.; Koschny, T.; Kafesaki, M.; Soukoulis, C. M. A Comparison of Graphene, Superconductors and Metals as Conductors for Metamaterials and Plasmonics. *Nat. Photonics* **2012**, *6*, 259–264.
24. Li, Z. Q.; Henriksen, E. A.; Jiang, Z.; Hao, Z.; Martin, M. C.; Kim, P.; Stormer, H. L.; Basov, D. N. Dirac Charge Dynamics in Graphene by Infrared Spectroscopy. *Nat. Phys.* **2008**, *4*, 532–535.
25. Peres, N. M. R.; Ribeiro, R. M.; Castro Neto, A. H. Excitonic Effect in the Optical Conductivity of Gated Graphene. *Phys. Rev. Lett.* **2010**, *105*, 055501.
26. Fei, Z.; Rodin, A. S.; Andreev, G. O.; Bao, W.; McLeod, A. S.; Wagner, M.; Zhang, L. M.; Zhao, Z.; Dominguez, G.; Thiemens, M.; *et al.* Gate-Tuning of Graphene Plasmons Revealed by Infrared Nano-imaging. *Nature* **2012**, *487*, 82–85.
27. Grushin, A. G.; Valenzuela, B.; Vozmediano, M. A. H. Effect of Coulomb Interactions on the Optical Properties of Doped Graphene. *Phys. Rev. B* **2009**, *80*, 155417.
28. Chen, J. N.; Badioli, M.; Alonso-González, P.; Thongrattanasiri, S.; Huth, F.; Osmond, J.; Spasenovic, M.; Centeno, A.; Pesquera, A.; Godignon, P.; *et al.* Optical Nano-Imaging of Gate-Tunable Graphene Plasmons. *Nature*, **2012**, DOI: 10.1038/nature11254.
29. Gannett, W.; Regan, W.; Watanabe, K.; Taniguchi, T.; Crommie, M. F.; Zettl, A. Boron Nitride Substrates for High Mobility Chemical Vapor Deposited Graphene. *Appl. Phys. Lett.* **2011**, *98*, 242105.
30. Wu, W.; Jauregui, L. A.; Su, Z.; Liu, Z.; Bao, J.; Chen, Y. P.; Yu, Q. Growth of Single Crystal Graphene Arrays by Locally Controlling Nucleation on Polycrystalline Cu Using Chemical Vapor Deposition. *Adv. Mater.* **2011**, *23*, 4898–4903.
31. Li, T.; Luo, L.; Hupalo, M.; Zhang, J.; Tringides, M. C.; Schmalian, J.; Wang, J. Femtosecond Population Inversion and Stimulated Emission of Dense Dirac Fermions in Graphene. *Phys. Rev. Lett.* **2012**, *108*, 167401.
32. Ryzhii, M.; Ryzhii, V. Injection and Population Inversion in Electrically Induced P-N Junction in Graphene with Split Gates. *Jpn. J. Appl. Phys.* **2007**, *46*, L151–L153.
33. Dragoman, D.; Dragoman, M; Plana, R. Tunable Electrical Superlattices in Periodically Gated Bilayer Graphene. *J. Appl. Phys.* **2010**, *107*, 044312.
34. Ruzicka, B. A.; Wang, S.; Werake, L. K.; Weintrub, B.; Loh, K. P.; Zhao, H. Hot Carrier Diffusion in Graphene. *Phys. Rev. B* **2010**, *82*, 195414.
35. Lee, W.; Degertekin, F. L. Rigorous Coupled-Wave Analysis of Multilayered Grating Structures. *J. Lightwave Technol.* **2004**, *22*, 2359–2363.
36. Christensen, J.; Manjavacas, A.; Thongrattanasiri, S.; Koppens, F. H. L.; de Abajo, F. J. G. Graphene Plasmon Waveguiding and Hybridization in Individual and Paired Nanoribbons. *ACS Nano* **2012**, *6*, 431–440.
37. Nikitin, A. Y.; Guinea, F.; Garcia-Vidal, F. J.; Martin-Moreno, L. Surface Plasmon Enhanced Absorption and Suppressed Transmission in Periodic Arrays of Graphene Ribbons. *Phys. Rev. B* **2012**, *85*, 081405.
38. Falkovsky, L. A. Optical Properties of Graphene. *J. Phys.: Conf. Ser.* **2008**, *129*, 012004.